analytical chemistry

Article

Cite This: *Anal. Chem.* 2018, 90, 12011−12018

pubs.acs.org/ac

Evaluation of a New Reagent-Ion Source and Focusing Ion−Molecule Reactor for Use in Proton-Transfer-Reaction Mass Spectrometry

Jordan Krechmer,[†,%] Felipe Lopez-Hilfiker,[‡,%] Abigail Koss,[§,∥,⊥,#] Manuel Hutterli,[‡] Carsten Stoermer,[‡] Benjamin Deming,[§,⊥] Joel Kimmel,[†,‡] Carsten Warneke,[§,∥] Rupert Holzinger,[¶] John Jayne,[†] Douglas Worsnop,[†] Katrin Fuhrer,[‡] Marc Gonin,[‡] and Joost de Gouw*[,§,⊥]

[†]Aerodyne Research Inc., Billerica, Massachusetts 01821, United States

[‡]TOFWERK AG, 3600 Thun, Switzerland

[§]Cooperative Institute for Research in Environmental Sciences, University of Colorado, Boulder, Colorado United States

[∥]Earth System Research Laboratory, NOAA, Boulder, Colorado 80305-3337, United States

[⊥]Department of Chemistry and Biochemistry, University of Colorado, Boulder, Colorado 80309, United States

[¶]Institute for Marine and Atmospheric Research, Utrecht University, 3584 CC Utrecht, The Netherlands

Supporting Information

ABSTRACT: We evaluate the performance of a new chemical ionization source called Vocus, consisting of a discharge reagent-ion source and focusing ion−molecule reactor (FIMR) for use in proton-transfer-reaction time-of-flight mass spectrometry (PTR-TOF) measurements of volatile organic compounds (VOCs) in air. The reagent ion source uses a low-pressure discharge. The FIMR consists of a glass tube with a resistive coating, mounted inside a radio frequency (RF) quadrupole. The axial electric field is used to enhance ion collision energies and limit cluster ion formation. The RF field focuses ions to the central axis of the reactor and improves the detection efficiency of product ions. Ion trajectory calculations demonstrate the mass-dependent focusing of ions and enhancement of the ion collision energy by the RF field, in particular for the lighter ions. Product ion signals are increased by a factor of 10 when the RF field is applied (5000−18 000 cps ppbv^{-1}), improving measurement precision and detection limits while operating at very similar reaction conditions as traditional PTR instruments. Because of the high water mixing ratio in the FIMR, we observe no dependence of the sensitivity on ambient sample humidity. In this work, the Vocus is interfaced to a TOF mass analyzer with a mass resolving power up to 12 000, which allows clear separation of isobaric ions, observed at nearly every nominal mass when measuring ambient air. Measurement response times are determined for a range of ketones with saturation vapor concentrations down to 5×10^4 μg m^{-3} and compare favorably with previously published results for a PTR-MS instrument.

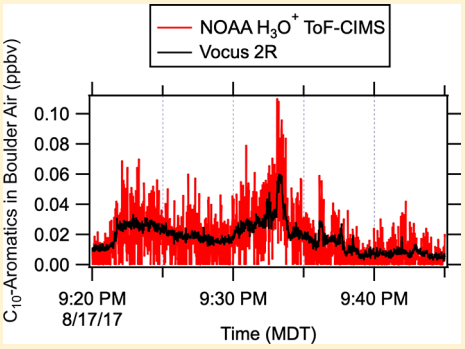

Proton-transfer-reaction mass spectrometry (PTR-MS) is a valuable tool for measurements of volatile organic compounds in air.[1] In PTR-MS, H_3O^+ ions are produced in a discharge ion source and ionize trace gases in the sample air by proton-transfer reactions in a drift tube reactor. The reagent and product ions are then detected with a mass spectrometer. The collision energy in a traditional PTR-MS is enhanced using a linear electric field, which is used to suppress cluster ion formation with water molecules and simplify the ion chemistry. The PTR-MS technique allows measurements of a broad range of trace gases including most volatile organic compounds (VOCs) in air with high sensitivity (parts-per-trillion by volume) and fast time response (<1 Hz).[1−4]

Since its invention, the PTR-MS technique has been improved in many significant ways. The original PTR-MS instruments used quadrupole mass analyzers, which were often used in selected-ion mode to improve measurement precision at the cost of comprehensiveness. Subsequent designs used time-of-flight (TOF) mass analyzers, which overcame the need to preselect the masses of interest before a measurement.[5−7] TOF mass analyzers with higher mass resolving power allowed the separation of isobaric ions, which significantly improved the analytical detail obtained.[8] Interfaces with quadrupole ion guides were used to improve the product-ion detection efficiency and lower the detection limits.[9,10]

Up until recently, the design of the reactor was relatively unchanged from the first PTR-MS instruments. In most instruments, a homogeneous electric field along the axial

Received: June 12, 2018
Accepted: September 16, 2018
Published: September 17, 2018

DOI: 10.1021/acs.analchem.8b02641
Anal. Chem. 2018, 90, 12011−12018

direction is used to enhance the ion kinetic energy and suppress cluster-ion formation. An added advantage is that the electric field transports the ions down the reactor, which reduces the need for large sample air flows and pumps. A disadvantage is that the reaction times are very short (~100 μs), which limits the net product ion formation. In the transverse direction, ions scatter and diffuse away from the central axis of the reactor. As the ion sampling orifice at the end of the reactor is small compared to the size of the ion beam, the detection efficiency of product ions is relatively low. Two recent instrument developments were aimed at overcoming these issues. First, ion funnels were introduced to collimate ions at the end of the reactor and improve detection efficiency.[11,12] A more radical redesign of the reactor was implemented in the PTR3 instrument, which is operated at a higher pressure (50−80 mbar), uses a tripole to enhance the ion kinetic energy, and relies on a large sampling flow to transport ions down the reactor, thereby allowing for much longer reaction times and more efficient product ion formation.[13]

Here, we evaluate the performance of a new reagent-ion source and focusing ion−molecule reactor (FIMR) developed by TOFWERK for use in PTR-MS. The FIMR uses a quadrupole RF field in the reactor to collimate ions onto the central axis and improve the detection efficiency, while maintaining approximately similar collision conditions used in conventional drift tubes. We describe the general design of the FIMR and evaluate the performance of an instrument that combines an FIMR with a time-of-flight mass spectrometer (TOFWERK Vocus 2R PTR-TOF; hereafter Vocus 2R). The operating principle of the FIMR is investigated using ion-trajectory calculations and laboratory characterization. We compare the performance of the Vocus 2R with a H_3O^+ ToF-CIMS instrument built at NOAA,[10] which uses a conventional drift tube and standard ion source but is otherwise very similar to the Vocus 2R. Finally, we investigate the response time of the system, which uses a short PEEK tube to introduce sample air into the reactor with important advantages over previously used inlets.[14]

INSTRUMENT DESCRIPTION

A schematic drawing of the Vocus is shown in Figure 1. Reagent ions are produced in a discharge ion source. The focusing ion−molecule reactor (FIMR) is composed of a glass tube with four quadrupole rods mounted radially on the outside. More detailed descriptions of the individual components follow below.

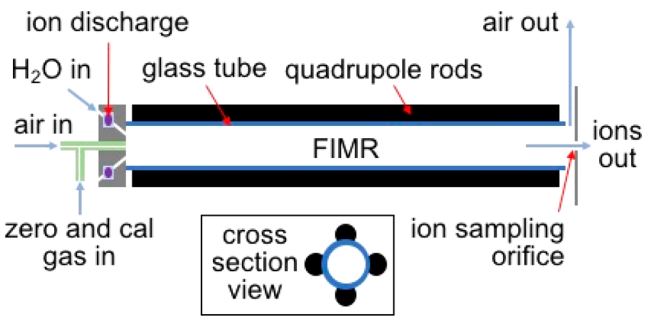

Figure 1. Design of the Vocus consisting of a discharge reagent-ion source and a focusing ion−molecule reactor (FIMR).

Reagent Ion Source. The reagent-ion source consists of two conical surfaces between which a plasma is produced. The design is different from the hollow-cathode ion sources used in most PTR-MS instruments. Water vapor from a reservoir (HPLC-grade or 18-MOhm milli-Q water) flows at 20−30 sccm (cm^3 min^{-1} at 10^5 Pa and 273.15 K) in between the surfaces, all of which enters the FIMR. A voltage of ~450 V discharges across the water vapor and the discharge current is regulated to ~1.5−2.0 mA, that is, the smallest value that still gives a stable ion signal. The discharge takes place in a ring around the central axis and ions enter the FIMR through a ring offset from the central axis. Photons generated by the discharge cannot directly enter the reactor. The water flow is optimized to yield the best reagent-ion signal distribution.

Focusing Ion−Molecule Reactor. Sample air enters the FIMR through a short (10 mm) PEEK tube with an internal diameter of 0.18 mm that acts as a pressure restriction similar to a critical orifice. The FIMR was operated at pressures of 1.0−1.5 mbar in this work. At these pressures, the sample flow is approximately 100 sccm. A larger diameter inlet tube allows a larger flow of air (e.g., 5 LPM) to be drawn to the entrance of the Vocus to reduce inlet wall losses and sampling delays. Only 100 sccm of this flow is sampled into the FIMR and the remainder is directed to the sample pump. Also orthogonal to the flow direction is a small port through which calibration and/or VOC-free air can be injected. This allows for fast and frequent calibrations and zeroing of the instrument while not perturbing the inlet line or sampling conditions (Figure S1).

The FIMR consists of a 10 cm long glass tube with an outside diameter of 13 mm and a glass thickness of 1.5 mm. The tube has a resistive coating on the inside surface, which forms a more homogeneous electric field than a stacked ring-electrode approach.[15] A DC voltage across the ends of the glass tube (typically ~500 V in this work) establishes the axial electric field in the reactor. Resistive glass tubes have been used previously as a reactor in other PTR-MS instruments[16,17] but with key differences to the approach used here. The Vocus uses four rods (6 mm diameter) mounted radially on the outside of the resistive glass tube, which are used to establish a quadrupole RF field inside to collimate ions into a narrow beam. At the end of the FIMR, ions are sampled into the TOF mass analyzer through a 2 mm diameter pinhole. The RF frequency is 1.3−1.6 MHz and is operated with an amplitude up to 600 Vpp.

The FIMR is pumped by a mechanical pump (390 L min^{-1} at 1 mbar), which is also used to back the turbo pump (Pfeiffer Split Flow 270) that is employed for the differentially pumped interface and the TOF mass analyzer. The reactor pressure is controlled by a valve between the reactor and mechanical pump. The pressure of the drift tube remains stable enough over time for laboratory or ground site measurements without intervention (Figure S2). A pressure controller is added for applications where sample pressure changes are significant.

Interface and Time-of-Flight Mass Analyzer. In the Vocus 2R, the FIMR is coupled to an API-TOF mass spectrometer[18,19] with two important changes: (i) the API-TOF is operated without the small segmented quadrupole that serves as an intermediate pressure stage in higher pressure chemical ionization systems and (ii) the Vocus 2R employs a mass analyzer from TOFWERK with a longer flight tube (nominal resolving power 10 000 Th/Th fwhm). Ions from the FIMR travel first into a big segmented quadrupole (BSQ) ion guide operated at 7×10^{-3} mbar to focus the ion beam before

DOI: 10.1021/acs.analchem.8b02641
Anal. Chem. 2018, 90, 12011−12018

entering the primary beam (PB) region and finally into the time-of-flight chamber held at 1×10^{-6} mbar. The TOF was configured to measure a mass-to-charge range of ~1−500 Th (16 kHz extraction frequency) for the experiments described herein.

Ion Trajectory Calculations. While the RF field adds a time-varying electric field, this field is zero along the central axis where the ion density is highest, and the average collision conditions are mostly dictated by the axial DC field as in conventional drift tubes. The average ion velocity v_{ion} in the axial direction is given by

$$v_{ion} = K \times E = K_0 \times (p_0/p) \times (T/T_0) \times E = K_0 \times N_0 \times E/N \quad (1)$$

where K is the ion mobility, E the electric field strength, and N the number density of gas in the FIMR. The reduced electric field strength, E/N, is a quantity describing the velocity and collision energy of the ions. The ion mobility under standard conditions ($p_0 = 1.013 \times 10^5$ Pa, $T_0 = 273.15$ K, and $N_0 = 2.69 \times 10^{19}$ cm^{-3}), or reduced ion mobility K_0, has been reported as 2.76 cm^2 V^{-1} s^{-1} for H_3O^+ ions in nitrogen.[20] Using K_0 and the operating conditions in the FIMR (p = 1.25 mbar, T = 298 K, and E = 50 V cm^{-1}), the residence time of ions is calculated to be 82 μs, which allows for ~120 cycles of the RF field before ions exit the reactor.

At a pressure of 1.25 mbar, the ion collision frequency of H_3O^+ reagent ions is around 28 MHz (assuming a collision rate coefficient with N_2 of 9×10^{-10} cm^3 molecule^{-1} s^{-1}).[21] This is a higher frequency than that of the RF (1.5 MHz) and therefore reagent ions will undergo many collisions during each RF cycle. It is therefore expected that the collision energy of the ions will vary at the frequency of the RF field, and that cluster formation and fragmentation can occur on each RF cycle.

Electric fields and ion trajectories in the FIMR were simulated using the software package SIMION (Scientific Instrument Services Inc.) and results are presented in Figure 2. A total of 10 000 trajectories were calculated in each case, with the Trajectory Quality parameter, which determines the time step and convergence of the calculations, set to 100. A smaller number of trajectories (1000) were also run at a higher Trajectory Quality parameter of 300 and gave very similar results. The pressure in the Vocus was set to 1.25 mbar. The axial electric field was set to 50 V cm^{-1} and simulations were run with and without a radial RF voltage (frequency 1.65 MHz; amplitude 400 Vpp) to show the focusing effect. The effects of collisions were simulated using a hard-sphere collision model. Hard-sphere collision cross sections for the $H_3O^+(H_2O)_n$ cluster ions were estimated from their ion mobilities[20] (H_3O^+ 47.6 Å^2, $H_3O^+(H_2O)$ 60.6 Å^2, $H_3O^+(H_2O)_2$ 64.7 Å^2). For product ions at 100 Th, we used a collision cross section of 98 Å^2 by extrapolation from the previous values. Not included in the trajectory calculations is the possible effect of space charges near the central axis.

Figure 2 shows the mean radial positions of ions of three different mass-to-charge values (19, 55, and 100 Th) with and without the RF voltage (RF amplitude equals 0 or 400 V). Ions are injected into the FIMR as a ring with a radius of 1.5 mm around the central axis, so all trajectories and their means start at that radius. Figure 2A shows that without the RF voltage, the ions spread out radially with the lighter ions forming a wider beam than heavier ions. A large part of the ion beam will not

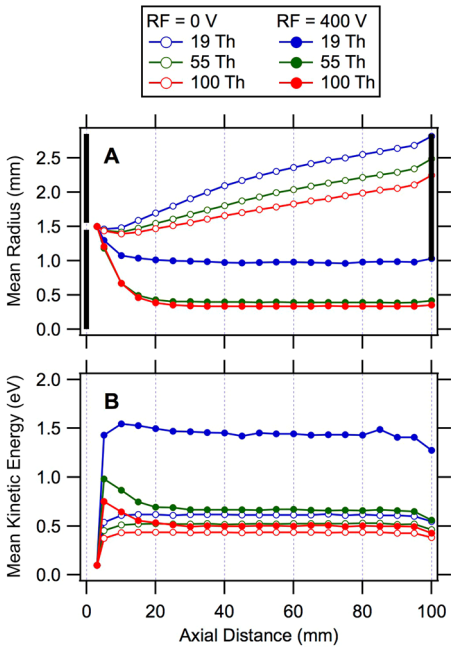

Figure 2. Results of trajectory calculations by SIMION for H_3O^+ (19 Th), $H_3O^+(H_2O)_2$ (55 Th), and product ions at 100 Th. Panel (A) shows the mean radius of the trajectories with and without the RF voltage as a function of the axial distance. The black, vertical lines show the geometry of the annual ion source and the sampling orifice of the Vocus. Panel (B) shows the mean kinetic energy of the modeled ions with and without the RF voltage.

be sampled by the 2 mm pinhole. Figure 2A shows that with an RF amplitude of 400 V, the mean ion trajectories are collimated toward the central axis. The focusing is the least efficient for the H_3O^+ ions, but the mean radius of the beam is still ~1 mm, which is the same as the size of the sampling orifice. Figure S3 illustrates the radial distribution of ions at the end of the FIMR with and without an RF amplitude of 400 V. Table S1 summarizes the fraction of the ion trajectories in the simulation that pass through the sampling orifice. The focusing effect of the RF field enhances the ion transmission by a factor of 7 to 9, which results in transmission efficiencies ranging from 54% for H_3O^+ to 99% for ions with a mass-to-charge of 100 Th. An added advantage of the RF field is that the residence time of the H_3O^+ reagent ions in the FIMR becomes 39% longer (Table S1). We attribute this to the higher average collision energy, which leads to a larger loss of ion velocity in the axial direction. Combined with the more efficient transmission of product ions, an overall increase in the product ion signals of more than an order of magnitude is achieved.

Figure 2 also shows the average ion kinetic energies of the three different ions with and without an RF field. Without the RF field, all ions reach a constant average kinetic energy after about ~10 mm of travel (Figure 2B). The kinetic energies are similar for the different ions, with the H_3O^+ ions reaching the highest mean energy. With an RF amplitude of 400 V, the ion kinetic energy is enhanced (Figure 2B). While the electric field along the central axis is only determined by the axial voltage, the time-varying electric field in the radial direction adds to the axial component of the electric field. As a result, the average ion kinetic energy increases with the radial distance. The H_3O^+ ions move on average further from the central axis, and their enhancement in kinetic energy is larger than for the heavier

DOI: 10.1021/acs.analchem.8b02641
Anal. Chem. 2018, 90, 12011−12018

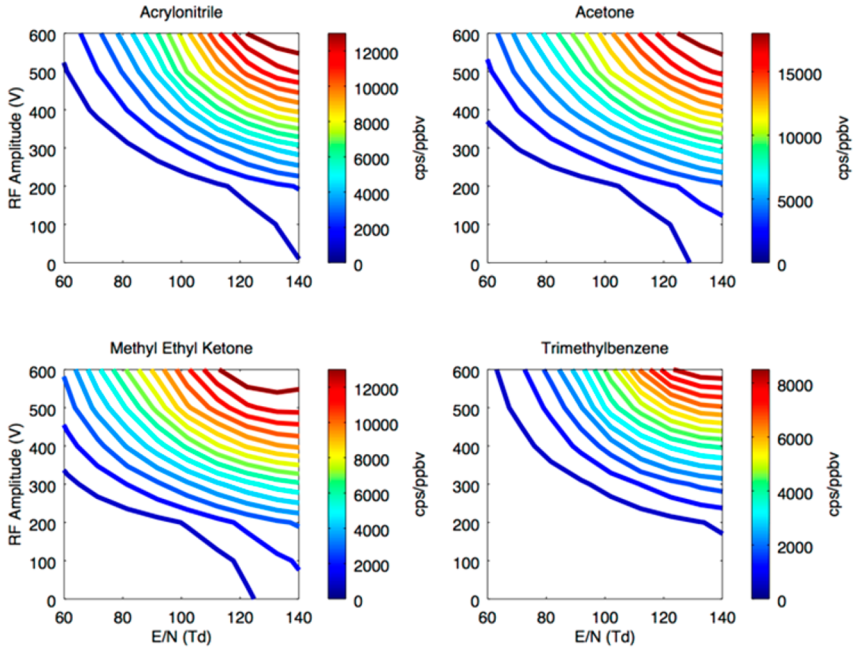

Figure 3. Product ion signals for acrylonitrile, acetone, methylethylketone, and trimethylbenzene as a function of axial voltage and RF amplitude. Mixing ratios of all VOCs were ~20 ppbv in these experiments.

ions. This illustrates a beneficial feature of the FIMR: the H_3O^+ ions are more efficiently heated than heavier ions by the RF field, which prevents the formation of water cluster ions, so that proton transfer from H_3O^+ is favored over switching reactions with $H_3O^+(H_2O)$. The product ions are better collimated to the central axis, where their kinetic energy is less enhanced by the RF field. This limits the fragmentation of product ions.

RESULTS AND DISCUSSION

Reagent ions and Instrument Response. Due to the focusing effect of the RF fields, the signal intensities for the H_3O^+ and $H_3O^+(H_2O)$ reagent ions are very high in the Vocus 2R and would quickly degrade the microchannel plate detector. To prevent this, the BSQ is set up as a high-pass band filter, whereby ions <35 Th are detected at a much-reduced efficiency. This is illustrated in quantitative detail in Figure S4. As a result, the actual distribution of $H_3O^+(H_2O)_n$ reagent ions in the FIMR is not the same as the measured distribution, which complicates the interpretation of the ion chemistry and the normalization of the measured signals to the changing reagent ion signals.

To illustrate the response of the Vocus 2R with regard to different VOCs, Figure 3 shows the product ion signals for four VOCs as a function of the axial voltage and RF amplitude. It is seen that the signals increase with both the axial voltage and RF amplitude. The RF fields enhance the ion detection efficiencies as shown above. A higher axial voltage reduces the residence time of ions in the FIMR and therefore limits the loss of ions by radial diffusion. In addition, the axial voltage determines the mean collision energy and therefore degree of $H_3O^+(H_2O)_n$ cluster ion formation. While acetone reacts efficiently with all $H_3O^+(H_2O)_n$ cluster ions, aromatics have been shown to react less efficiently with $H_3O^+(H_2O)_n$ ions.[2] This explains why the acetone signal is observed over a broader range in axial voltages.

The FIMR is operated at a relatively high axial reduced field strength (148×10^{-17} V cm^2 = 148 Townsend) at a pressure of 1.25 mbar and electric field of 45 V cm^{-1}. This is higher than the typical values of 100−120 Townsend used in PTR-MS.[2] Part of the reason that a higher value of E/N is needed to decluster the reagent ions is the high mixing ratio of water in the FIMR (~20%). Also, the addition of this lighter gas to the sample flow lowers the collision energy and effectively decreases the mobility in the N_2−O_2-H_2O mixture,[22] which even further lowers the ion velocity and collision energy. At these values of E/N, the $H_3O^+(H_2O)_n$ reagent ion distribution is dominated by H_3O^+ ions[2] (Figure S5). Fragmentation of product ions is not strongly enhanced by the RF field (Figures S6 and S7). Based on the count rate of acetone product ions (300 000 cps) at their sampled mixing ratio of 20 ppbv, the H_3O^+ count rate can be calculated to be >10^9 cps. This is much higher than the measured count rate due to the mass discrimination effect of the BSQ.

The discharge ion source can also generate radicals such as hydroxyl (OH). To test if OH reactions with reactive VOCs in the FIMR can lead to detection of spurious products, we added high concentrations of isoprene and α-pinene to the instrument (Figure S8). No significant OH reaction products such as pinonaldehyde were detected. Other ions such as NO^+ and O_2^+ have typically 3 and 1 orders of magnitude lower signals than $H_3O^+(H_2O)$. For the Vocus 2R used here, the ratio between charge-transfer and proton-transfer reactions was determined to be 2.2% for α-pinene (M^+/MH^+ = 2.2%), and 6.1% for isoprene (M^+/MH^+ = 6.1%).

Sensitivity. The Vocus 2R was deployed in the field during the PICAB campaign (PTR-MS Intercomparison campaign at CABauw) that was conducted in 2017 in the framework of ACTRIS (European Research Infrastructure for the observation of Aerosol, Clouds, and Trace gases). A comparison of the different PTR-MS measurements involved will be presented elsewhere. Here, we focus on the results of the calibration measurements.

DOI: 10.1021/acs.analchem.8b02641
Anal. Chem. 2018, 90, 12011−12018

Automated gas-phase calibrations of the Vocus 2R instrument were performed every 2 h by injecting a measured concentration of a multicomponent gas-phase standard from a prepared cylinder (Apel-Riemer Environmental). The gas calibrant was diluted into VOC-free air produced by flowing ambient air through a hydrocarbon trap (VICI). The results of 24 h of calibrations for several atmospheric VOCs are summarized in Table S2 and are compared in Figure 4A with published values from the NOAA H_3O^+ ToF-CIMS instrument.[23−25] The sensitivities of the two instruments correlate well with each other (r^2 = 0.885), with the exception of acetonitrile and acetaldehyde, which are partially cut off by the BSQ (see Figure S4). The slope of a linear regression fit through these data points (excluding acetonitrile and acetaldehyde) shows that the Vocus 2R is ∼19 times more sensitive than the H_3O^+ ToF-CIMS instrument. These two instruments differ in two important ways: (i) a conventional drift tube reactor in the H_3O^+ ToF-CIMS vs the FIMR in the Vocus 2R, and (ii) a TOFWERK HTOF mass analyzer in the H_3O^+ ToF-CIMS vs a TOFWERK LTOF mass analyzer in the Vocus 2R. The enhancement in sensitivity is very similar to the enhancement calculated from ion trajectories in SIMION, which suggests that a defocusing effect from space charge near the central axis is not large. Acetaldehyde is detected about 3 times more sensitively, and acetonitrile has about the same sensitivity as the H_3O^+ ToF-CIMS instrument at these BSQ settings. Depending on the mass spectral region of interest, these sensitivities can be improved by adjusting the bandpass window of the BSQ (Figure S4). The Vocus 2R sensitivities are at the upper end of the range for PTR-MS instruments as summarized elsewhere[4,10] and similar to the sensitivities of the PTR3 for oxygenated VOCs.[13] Results from a laboratory calibration using a different standard mixture are shown in Figure S9 and illustrate the linearity of the instrument response.

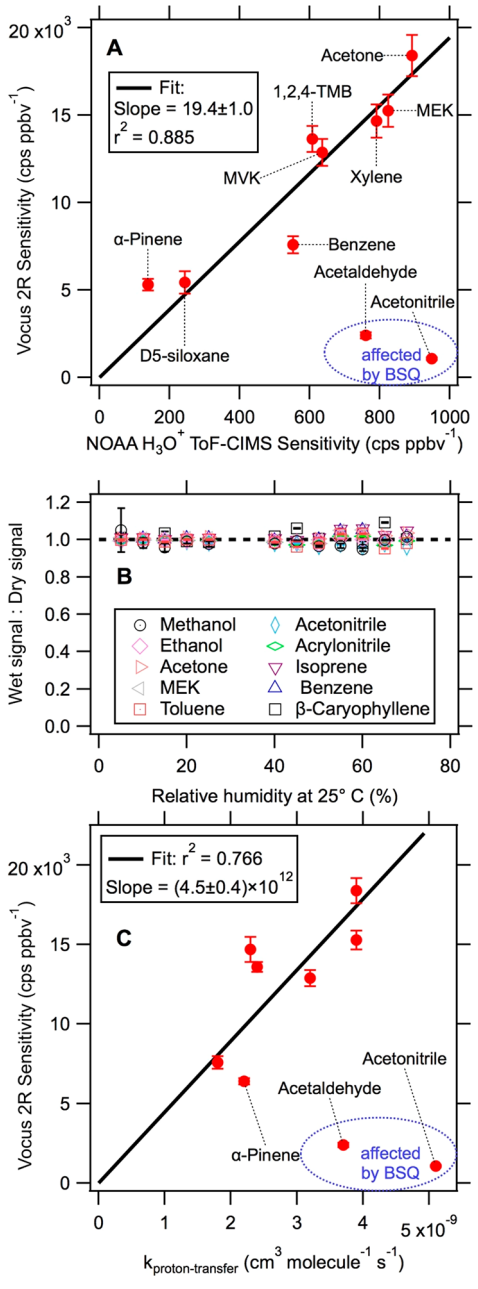

Figure 4. (A) Comparison of sensitivities between the Vocus 2R and the NOAA H_3O^+ ToF-CIMS. Vocus sensitivities were determined during the ACTRIS-PICAB field campaign and represent an average over 24 h (12 separate calibrations). Error bars represent the 1σ standard deviation. Sensitivities are reported for a 25 kHz extraction frequency. Sensitivities for the H_3O^+ ToF-CIMS for o-xylene,[23] D5-siloxane,[25] and other compounds[24] were taken from the literature. (B) Humidity dependence of the Vocus 2R product ion signals from a separate experiment. (C) Correlation between the Vocus 2R sensitivities and the proton-transfer reaction rate coefficients.

The Vocus 2R sensitivities for acetone and benzene were the same within a factor of 2−3 (Table S2). This confirms that H_3O^+ ions are the dominant reagent ions in the Vocus 2R, as benzene and other hydrocarbons do not react as efficiently with $H_3O^+(H_2O)$ ions.[2]

In contrast with conventional PTR sources,[2] the Vocus does not show a sensitivity dependence on the humidity of the sample air. To illustrate, Figure 4B shows the results of a calibration by mixing standard gas compounds into clean air that was humidified using a bubbler at room temperature. The temperature limited the maximum humidity to ∼75% RH and the increased scatter at high RH is due to fewer sampling points. This is due to the large mixing ratio of water vapor in the FIMR (∼ 20% by volume). Therefore, the humidity of the sample air has only a very small effect on ion−molecule reactions in the Vocus and thereby the sensitivity.

A specific advantage of PTR-MS is that the sensitivities for different VOCs can be calculated from the kinetics of the proton-transfer reactions.[23,26,27] We note here that the Vocus 2R is similar in this regard: Figure 4C shows the correlation between the sensitivities from Figure 4A and their proton-transfer rate coefficients. Using calibration standards, the relationship between sensitivity and reaction rate coefficient can be established and used to calculate the sensitivity for other compounds. More work is needed to study the sensitivity of the Vocus 2R given the time-varying effect of the RF field on the collision energy. In addition, the effects of back reactions between product ions and water vapor, which can reduce the sensitivity for compounds such as formaldehyde,[28] need to be studied in more detail.

Measurement Comparison. In August 2017, the Vocus 2R performance was characterized in a series of tests in the NOAA laboratories. Measurements of ambient air were made in parallel with the NOAA H_3O^+ ToF-CIMS.[10] Figure 5 shows a comparison of measurements of different aromatics in ambient air made by the two instruments. Both instruments

DOI: 10.1021/acs.analchem.8b02641
Anal. Chem. 2018, 90, 12011−12018

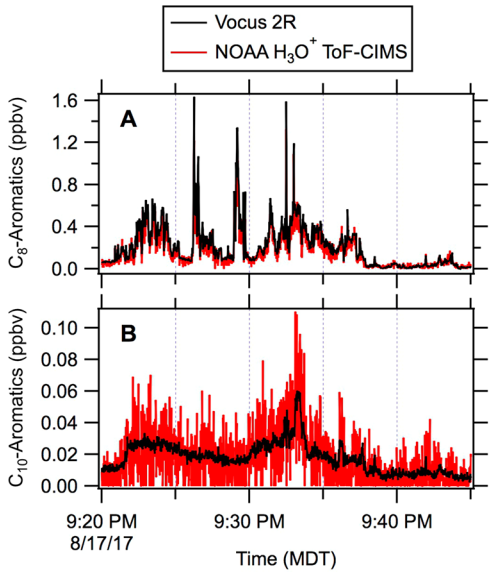

Figure 5. Comparison of measured time series of (A) C_8-aromatics and (B) C_{10}-aromatics in Boulder by the Vocus 2R and NOAA H_3O^+ ToF-CIMS instruments. Both instruments acquired data at 1 Hz and are compared on the same time base here (i.e., not smoothed). The Vocus 2R was not equipped with a catalytic converter for the determination of background mixing ratios. Instead a constant value was subtracted from each time series for the purpose of this comparison.

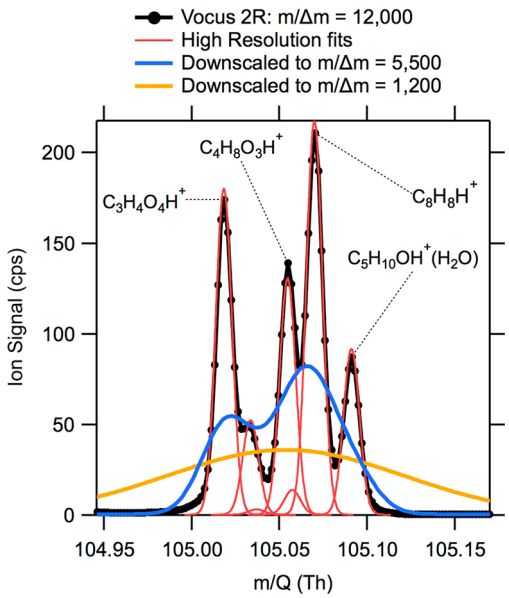

Figure 6. A mass spectrum of ambient air from one 2-Hz saved spectrum (24 September 2017, 18:48:34 UTC) at m/Q = 105 Th. With a mass resolving power $m/\Delta m$ = 12 000, five peaks were resolved in the deconvolution. The same mass spectrum was then down-sampled to lower resolving powers of 5500 and 1200.

were calibrated using the same standard mixture containing toluene, o-xylene and 1,2,4-trimethylbenzene. The sensitivity of the H_3O^+ ToF-CIMS to C_{10} aromatics was calculated from the kinetic rate constant, and the Vocus 2R sensitivity to C_{10} aromatics is estimated on the basis of the comparison. Both instruments measured at the same time resolution (1 Hz saved spectra).

Figure 5 shows that the Vocus 2R and H_3O^+ ToF CIMS show all of the same features for C_8- and C_{10}-aromatics, but the Vocus 2R measures with much higher precision due to its higher sensitivity. During the measurement period, the C_8-aromatics had enhancements above 1 ppbv and the two instruments agree well for these high signals. Mixing ratios of C_{10}-aromatics were below 100 pptv. The precision of the C_{10}-aromatics measurements was estimated from a brief period when there was no discernible structure in the signal. The 2σ-noise in the Vocus 2R data was 2 pptv and the 2σ-noise in the H_3O^+ ToF-CIMS data was 12 pptv. This improvement in precision by a factor of ~6 is as expected from the enhancement in sensitivity.[4]

Mass Spectral Resolution. Figure 6 shows a 2 Hz mass spectrum obtained during the ACTRIS-PICAB campaign at 105 Th. The full mass spectrum is provided in Figure S10. With a mass resolution $m/\Delta m$ = 12 000, the Vocus 2R resolved five peaks. Previous work has attributed the signal at 105 Th to styrene, which is indeed the largest peak ($C_8H_8H^+$). In photochemically aged air masses, peroxy isobutyryl nitrate or PiBN can also contribute to the signal as protonated peroxybutyric acid[29] ($C_4H_8O_3H^+$), which is the third largest peak in the spectrum. The other two peaks are possibly malonic acid ($C_3H_4O_4H^+$) and the water cluster of C_5-carbonyls ($C_5H_{10}OH^+(H_2O)$). Malonic acid may not have been identified previously due to its low volatility, which prevents it from passing efficiently through inlet tubing.[14]

At a theoretical mass resolving power $m/\Delta m$ = 5500 and 1200, the instrument would only detect two and one peak(s), respectively, as illustrated in Figure 6. This shows that the higher mass-resolving power of the Vocus 2R allows smaller signals to be quantified with higher precision, in addition to the higher measurement sensitivity.

Inlet Design and Time Response. Instrument time response is a critical parameter for many applications including eddy covariance fluxes,[30] breath analysis,[31] and measurements from mobile platforms.[32] Instrument response times for the Vocus 2R were determined from experiments with an 8 m^3 environmental chamber following procedures described previously.[14] Several ketones with varying vapor pressures were added to the chamber and allowed to equilibrate between the gas phase and the FEP chamber walls. Mixing ratios were approximately 20 ppbv and less for the compounds with lower saturation vapor concentration[33] C* that partition to the walls. The Vocus 2R was set up to sample from the chamber. After all ketones had reached a constant product ion signal, the inlet was abruptly removed from the critical orifice and the decrease in signal recorded (Figure 7). The decrease in signal versus time can be described by a double or triple exponential. The first 40–60% of the signal decreased within ~1 s for all compounds, which is attributed to the rapid clearing of the volume of the FIMR with laboratory air (marked as "fast" decrease in Figure 7).

The next fraction of the signal showed a slower decrease on a time scale of seconds to a minute that was different for each compound. We attribute this decrease (marked as "determined by C*" in Figure 7) as the partitioning of ketones from the walls of the inlet and FIMR to the sample air, which was previously shown[14] to be mostly determined by C*. In Figure S11, we compare the measurement delay times resulting from this effect with those from an earlier study with a PTR-MS instrument equipped with a pressure-controlled inlet. Importantly, these delay times in the Vocus 2R are about an order

DOI: 10.1021/acs.analchem.8b02641
Anal. Chem. 2018, 90, 12011–12018

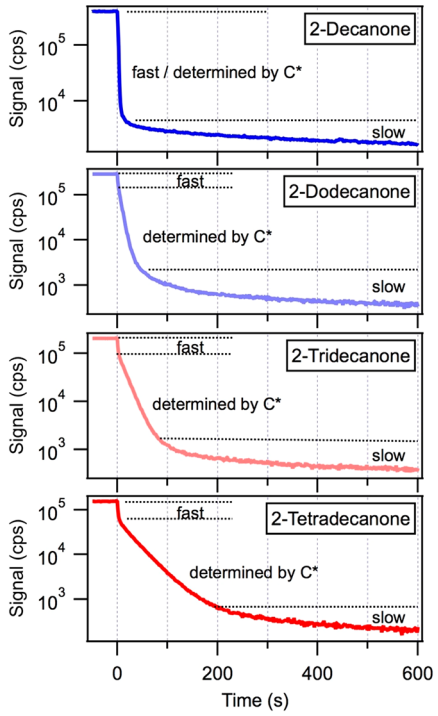

Figure 7. Decrease in the signal for four ketones after abruptly stopping the sampling from an environmental chamber equilibrated with these compounds. For 2-dodecanone through 2-tetradecanone, three phases can be distinguished in the time response. For 2-decanone, the fast decrease due to volume clearing and the decrease determined by C* occur at the approximate same rate and cannot be distinguished from each other.

of magnitude shorter than those obtained with the quadrupole PTR-MS.

The remaining fraction of the signal decreased at the same rate for all compounds (marked as "slow" in Figure 7). A potential explanation is the slow mixing out of sample gas trapped in dead spaces in the instrument. For all compounds, this slow decrease of the signal only concerns a very small fraction of the signal.

In summary, overall measurement response times in the Vocus 2R are better than 1 s for compounds with C* > 10^6 μg m^{-3}. Below 10^6 μg m^{-3}, a fraction of the signal decreases within ~1 s and another fraction decreases more slowly. At a lower C* than used in these experiments, one can expect that the decrease determined by C* becomes so slow that it is not important on the time scale of most measurements, making the effective response time on the order of seconds. This effect has been observed for chamber wall losses,[34] but needs to be verified for the Vocus 2R in future work.

Overall $1/e^2$ delay times for the ketones studied here ranged from 1 to 35 s. These results were obtained without heating the FIMR, which improves the delay times. Also, the effect of different materials in the FIMR can be investigated further. Instrument delay times for a high-temperature PTR-MS[35] were reported for semivolatile compounds such as levoglucosan, oxalic acid and cis-pinonic acid and ranged from 8 to 370 s depending on concentrations.

CONCLUSIONS

The design of the new Vocus annular ion source and focusing ion−molecule reactor for use in PTR-MS is described. Trajectory calculations and calibrations show that the use of RF fields improves the detection efficiency of ions produced from reactions between H_3O^+ reagent ions and VOCs by about an order of magnitude. The instrument sensitivity shows no dependence on ambient humidity. The Vocus is coupled to a TOF mass analyzer with a longer time-of-flight region, thereby achieving a mass resolving power of 12 000. The time response of the Vocus 2R instrument is characterized. At least ~50% of the signal decreases within seconds, whereas the remaining fraction decreases more slowly depending on the saturation vapor concentrations C* of the measured compounds.

The new Vocus chemical ionization source combined with the 2R time-of-flight mass analyzer allows fast measurements of VOCs at single pptv levels, with a higher mass resolution and shorter response times than previously demonstrated. Historically an important application of PTR-MS has been the measurements of atmospheric VOCs. The Vocus 2R will allow measurements of many more atmospheric VOCs, which will improve the quantitative separation of different emission sources. The Vocus 2R will allow measurements of VOC reaction products and intermediates, which are present in small concentrations and often difficult to measure because of partitioning to instrument surfaces.

Finally, this work demonstrated the use of H_3O^+ as the reagent ion, but we note that the Vocus chemical ionization source can also be operated with other ions, which can further expand its capabilities.

ASSOCIATED CONTENT

Supporting Information

The Supporting Information is available free of charge on the ACS Publications website at DOI: 10.1021/acs.analchem.8b02641.

Sampling efficiencies and residence times of different ions, average Vocus 2R sensitivities for selected VOCs measured during the ACTRIS-PICAB field campaign and the 1σ-variability from the individual calibrations, time series of a 2-minute-long background measurement obtained by the Vocus 2R during the ACTRIS-PICAB field campaign, and other data as mentioned in the text (PDF)

AUTHOR INFORMATION

Corresponding Author

*E-mail: Joost.deGouw@colorado.edu.

ORCID

Joost de Gouw: 0000-0002-0385-1826

Present Address

#A.K.: Massachusetts Institute of Technology, Cambridge, Massachusetts 02139, United States.

Author Contributions

%These authors contributed equally

Notes

The authors declare the following competing financial interest(s): Felipe Lopez-Hilfiker, Manuel Hutterli, Carsten Stoermer, Joel Kimmel, Katrin Fuhrer and Marc Gonin are employees of TOFWERK, which has developed and commercialized the Vocus PTR-TOF. Jordan Krechmer, John Jayne, Joel Kimmel and Douglas Worsnop are employees of Aerodyne Research Inc., which has partnered with TOFWERK to develop and commercialize atmospheric

DOI: 10.1021/acs.analchem.8b02641
Anal. Chem. 2018, 90, 12011−12018

chemistry research applications of the Vocus PTR-TOF. Joost de Gouw worked as a part-time consultant for Aerodyne Research Inc. during this project.

■ ACKNOWLEDGMENTS

The Authors are grateful to Paul Ziemann for the response time experiments performed in his laboratory and to Demetrios Pagonis and Jose-Luis Jimenez for useful discussions about the method. This manuscript is part of a project that has received funding from the European Union's Horizon 2020 research and innovation program under grant agreement no. 654109.

■ REFERENCES

(1) Lindinger, W.; Hansel, A.; Jordan, A. *Int. J. Mass Spectrom. Ion Processes* **1998**, *173* (3), 191−241.
(2) de Gouw, J. A.; Warneke, C. *Mass Spectrom. Rev.* **2007**, *26*, 223−257.
(3) Blake, R. S.; Monks, P. S.; Ellis, A. M. *Chem. Rev.* **2009**, *109*, 861−896.
(4) Yuan, B.; Koss, A. R.; Warneke, C.; Coggon, M.; Sekimoto, K.; de Gouw, J. A. *Chem. Rev.* **2017**, *117* (21), 13187−13229.
(5) Blake, R. S.; Whyte, C.; Hughes, C. O.; Ellis, A. M.; Monks, P. S. *Anal. Chem.* **2004**, *76* (13), 3841−3845.
(6) Inomata, S.; Tanimoto, H.; Aoki, N.; Hirokawa, J.; Sadanaga, Y. *Rapid Commun. Mass Spectrom.* **2006**, *20*, 1025−1029.
(7) Jordan, A.; Haidacher, S.; Hanel, G.; Hartungen, E.; Märk, L.; Seehauser, H.; Schottkowsky, R.; Sulzer, P.; Märk, T. D. *Int. J. Mass Spectrom.* **2009**, *286*, 122−128.
(8) Graus, M.; Müller, M.; Hansel, A. *J. Am. Soc. Mass Spectrom.* **2010**, *21* (6), 1037−1044.
(9) Sulzer, P.; Hartungen, E.; Hanel, G.; Feil, S.; Winkler, K.; Mutschlechner, P.; Haidacher, S.; Schottkowsky, R.; Gunsch, D.; Seehauser, H.; Striednig, M.; Jürschik, S.; Breiev, K.; Lanza, M.; Herbig, J.; Märk, L.; Märk, T. D.; Jordan, A. *Int. J. Mass Spectrom.* **2014**, *368*, 1−5.
(10) Yuan, B.; Koss, A. R.; Warneke, C.; Gilman, J. B.; Lerner, B. M.; Stark, H.; de Gouw, J. A. *Atmos. Meas. Tech.* **2016**, *9*, 2735−2752.
(11) Barber, S.; Blake, R. S.; White, I. R.; Monks, P. S.; Reich, F.; Mullock, S.; Ellis, A. M. *Anal. Chem.* **2012**, *84*, 5387−5391.
(12) Brown, P. A.; Cristescu, S. M.; Mullock, S. J.; Reich, D. F.; Lamont-Smith, C. S.; Harren, F. J. M. *Int. J. Mass Spectrom.* **2017**, *414*, 31−38.
(13) Breitenlechner, M.; Fischer, L.; Hainer, M.; Heinritzi, M.; Curtius, J.; Hansel, A. *Anal. Chem.* **2017**, *89*, 5824−5831.
(14) Pagonis, D.; Krechmer, J. E.; de Gouw, J. A.; Jimenez, J. L.; Ziemann, P. J. *Atmos. Meas. Tech.* **2017**, *10*, 4687−4696.
(15) Kaplan, K.; Graf, S.; Tanner, C.; Gonin, M.; Fuhrer, K.; Knochenmuss, R.; Dwivedi, P.; Hill, H. H., Jr. *Anal. Chem.* **2010**, *82* (22), 9336−9343.
(16) Thornberry, T.; Murphy, D. M.; Thomson, D. S.; de Gouw, J. A.; Warneke, C.; Bates, T. S.; Quinn, P. K.; Coffman, D. *Aerosol Sci. Technol.* **2009**, *43*, 486−501.
(17) Mikoviny, T.; Kaser, L.; Wisthaler, A. *Atmos. Meas. Tech.* **2010**, *3* (3), 537−544.
(18) Junninen, H.; Ehn, M.; Petaja, T.; Luosujärvi, L.; Kotiaho, T.; Kostiainen, R.; Rohner, U.; Gonin, M.; Fuhrer, K.; Kulmala, M.; Worsnop, D. R. *Atmos. Meas. Tech.* **2010**, *3* (4), 1039−1053.
(19) Bertram, T. H.; Kimmel, J. R.; Crisp, T. A.; Ryder, O. S.; Yatavelli, R. L. N.; Thornton, J. A.; Cubison, M.; Gonin, M.; Worsnop, D. R. *Atmos. Meas. Tech.* **2011**, *4* (7), 1471−1479.
(20) Dotan, I.; Albritton, D. L.; Lindinger, W.; Pahl, M. *J. Chem. Phys.* **1976**, *65*, 5028−5030.
(21) Gioumousis, G.; Stevenson, D. P. *J. Chem. Phys.* **1958**, *29* (2), 294−299.
(22) de Gouw, J. A.; Krishnamurthy, M.; Leone, S. R. *J. Chem. Phys.* **1997**, *106* (14), 5937−5942.
(23) Sekimoto, K.; Li, S.-M.; Yuan, B.; Koss, A. R.; Coggon, M.; Warneke, C.; de Gouw, J. A. *Int. J. Mass Spectrom.* **2017**, *421*, 71−94.
(24) Koss, A. R.; Sekimoto, K.; Gilman, J. B.; Selimovic, V.; Coggon, M. M.; Zarzana, K. J.; Yuan, B.; Lerner, B. M.; Brown, S. S.; Jimenez, J. L.; Krechmer, J. E.; Roberts, J. M.; Warneke, C.; Yokelson, R. J.; de Gouw, J. A. *Atmos. Chem. Phys.* **2018**, *18*, 3299−3319.
(25) Coggon, M. M.; McDonald, B. C.; Vlasenko, A.; Veres, P. R.; Bernard, F.; Koss, A. R.; Yuan, B.; Gilman, J. B.; Peischl, J.; Aikin, K. C.; DuRant, J.; Warneke, C.; Li, S.-M.; de Gouw, J. A. *Environ. Sci. Technol.* **2018**, *52*, 5610−5618.
(26) Warneke, C.; de Gouw, J. A.; Kuster, W. C.; Goldan, P. D.; Fall, R. *Environ. Sci. Technol.* **2003**, *37* (11), 2494−2501.
(27) Cappellin, L.; Karl, T.; Probst, M.; Ismailova, O.; Winkler, P. M.; Soukoulis, C.; Aprea, E.; Märk, T. D.; Gasperi, F.; Biasioli, F. *Environ. Sci. Technol.* **2012**, *46* (4), 2283−2290.
(28) Vlasenko, A.; Macdonald, A. M.; Sjostedt, S. J.; Abbatt, J. P. D. *Atmos. Meas. Tech.* **2010**, *3* (4), 1055−1062.
(29) de Gouw, J. A.; Goldan, P. D.; Warneke, C.; Kuster, W. C.; Roberts, J. M.; Marchewka, M.; Bertman, S. B.; Pszenny, A. A. P.; Keene, W. C. *J. Geophys. Res.-Atmos.* **2003**, *108* (D21), 4682.
(30) Karl, T.; Guenther, A. B.; Lindinger, C.; Jordan, A.; Fall, R.; Lindinger, W. *J. Geophys. Res.-Atmos.* **2001**, *106* (D20), 24157−24167.
(31) Trefz, P.; Schmidt, M.; Oertel, P.; Obermeier, J.; Brock, B.; Kamysek, S.; Dunkl, J.; Zimmermann, R.; Schubert, J. K.; Miekisch, W. *Anal. Chem.* **2013**, *85* (21), 10321−10329.
(32) Karl, T.; Apel, E. C.; Hodzic, A.; Riemer, D. D.; Blake, D. R.; Wiedinmyer, C. *Atmos. Chem. Phys.* **2009**, *9*, 271−285.
(33) Donahue, N. M.; Robinson, A. L.; Stanier, C. O.; Pandis, S. N. *Environ. Sci. Technol.* **2006**, *40* (8), 2635−2643.
(34) Krechmer, J. E.; Pagonis, D.; Ziemann, P. J.; Jimenez, J. L. *Environ. Sci. Technol.* **2016**, *50* (11), 5757−5765.
(35) Mikoviny, T.; Kaser, L.; Wisthaler, A. *Atmos. Meas. Tech.* **2010**, *3* (3), 537−544.

DOI: 10.1021/acs.analchem.8b02641
Anal. Chem. 2018, 90, 12011−12018